REVISTA IBRACON DE ESTRUTURAS E MATERIAIS

IBRACON STRUCTURES AND MATERIALS JOURNAL

Weighing in motion and characterization of the railroad traffic with using the B-WIM technique

Pesagem em movimento e caracterização do tráfego ferroviário com uso da técnica B-WIM

J. A. DE CARVALHO NETO [a]
decarvalho@ufpa.br

L. A. C. M. VELOSO [a]
lveloso@ufpa.br

Abstract

The knowledge on the active moving load of a bridge is crucial for the achievement of the information on the behavior of the structure, and thus foresee maintenance, repairs and better definition of the logistics of its active vehicles. This paper presents the development of the algorithms for the application of the Bridge-Weigh In Motion (B-WIM) method created by Moses for the weighing of trains during motion and also for the characterization of the rail traffic, allowing the obtainment of information like passage's train velocity and number and spacing of axles, eliminating the dynamic effect. There were implemented algorithms for the determination of the data referring to the geometry of the train and its loads, which were evaluated using a theoretical example, in which it was simulated the passage of the train over a bridge and the loads of its axles were determined with one hundred percent of precision. In addition, it was made a numerical example in finite elements of a reinforced concrete viaduct from the Carajás' Railroad, in which the developed system reached great results on the characterization and weighing of the locomotive when the constitutive equation of the Brazilian Standards was substituted by the one proposed by Collins and Mitchell.

Keywords: B-WIM, axle loads, bridges, numerical modeling, gross vehicle weight.

Resumo

O conhecimento do carregamento móvel atuante em uma ponte é de grande importância para obter a informação do comportamento da estrutura, e assim prever manutenção, reparos e definir melhor a logística dos veículos que circulam sob a mesma. Este trabalho apresenta o desenvolvimento dos algoritmos para aplicação do método Bridge-Weigh In Motion (B-WIM) criado por MOSES (1979) para a pesagem em movimento de trens e também para a caracterização do tráfego ferroviário, permitindo-se obter informações sobre a velocidade de passagem dos trens, número e espaçamento entre eixos, eliminando o efeito dinâmico. Foram implementados os algoritmos para a determinação dos dados referentes a geometria do trem e das cargas, que foi validado a partir de um exemplo teórico, onde se simulou a passagem do trem sobre a ponte e as cargas por eixos foram determinadas com 100% de exatidão. Além disso, foi feito um exemplo numérico em elementos finitos, de um viaduto em concreto armado para aplicações do método, onde foi feita a determinação das cargas por eixo para diferentes velocidades de passagem do trem. Finalmente, o método foi testado em um caso real a partir de monitorações realizadas em um viaduto de concreto armado da Estrada de Ferro Carajás, onde o sistema desenvolvido conseguiu atingir ótimos resultados na caracterização e pesagem da locomotiva quando se substituiu a equação constitutiva da ABNT NBR 6118 (2007) pela equação proposta por Collins e Mitchell (1991).

Palavras-chave: B-WIM, carga por eixo, pontes, modelo numérico, peso bruto total.

1. Introduction

The studies on railroad bridges have led to great improvements regarding the understanding of their dynamic behavior. Furthermore, many researches are carried aiming the evaluation of the real characteristics of its active traffic.

Every structure must be conceived and designed so that it is able to support, with an appropriate margin of safety, the loads and deformations predicted during its operating life. In this context, there is a special interest on the development of methodologies that allow the measurement of the real effects of the traffic on the railroad's structures, in a manner that, in the future, to be possible, in a relatively simple way, to increase the axle loads and speed of traffic, with no need of big investments in infrastructure.

The acquisition of information on the axles and gross weight of the vehicles have been object of studies around the world since the 70's, having their origin in a research which took place in a road bridge near Cleveland, Ohio (Moses [1]). This kind of data is essential in the design of new structures and maintenance of old bridges and viaducts.

The weigh-in-motion methods were created to determine the axle's loads and gross weight of vehicles during highway trips, avoiding the vehicles to stop. These methods were called Weigh-In-Motion (WIM) and divided in two categories based on the type of instrumentation used, which could be assembled on the pavement (WIM) or in bridges (Bridge Weigh-In-Motion – B-WIM) (Moses[1]), see Figure [1].

2. Experimental determination of moving loads (Moses' algorithm)

Studies on the loads of traffic are a normal practice in respect of road traffic worldwide. The fact comes from the great expansion of the road transport of goods in the second half of the twentieth century. It was verified that the recent growth of the loads transported by vehicles led to the deterioration of the pavements and bridges, what induced the need of control of these loads. Initially, the control was done through static weighing systems. Despite their high precision, the reduced number of heavy vehicles, as well as the delay caused by the process, increased the interest on the development of dynamic methods of weighing.

In order to satisfy the necessity of studying the traffic load on roads, were developed many systems of weighing during motion, which take measurements through sensors installed on the pavement. These systems can determine with high precision the load of vehicles.

The B-WIM differs from other systems due the use of measurements of deformation from the bridges, not the pavement, during the passage of vehicles. The advantage of this system is that it allows the weighing along the length of the bridge, while the others weigh a single lane of the pavement. Moreover, it is possible to filter the signal to take the dynamic effect caused by flaws in the wheels and irregularities on the lane. The method can be applied both in characterization of the traffic of highways and railroads.

The characteristics of the structures in which the B-WIM algorithms will be used have particular significance for obtaining good results, specially the length of the free span and the dynamic properties of the structure (Pimentel [4]). The bridges of short free span are more frequently used in the application of the algorithm, once a large free span bridge would have several axles acting on the same span, condition that would forbid the determination of the load per axle, but permits to detect the trucks with better precision.

Regarding the dynamic properties of these bridges, the dynamic effects due the passage of the train must be filtered, so the frequencies of the vehicles, derived from the relation between the velocity (which must be constant) and their axle's spacing, see Equation [1], are isolated. The feature that makes these structures able

Figure 1 – WIM methods: a) Measurements on the pavement, WIM; b) B-WIM, complete system (Znidaric e Baumgärtner, (2) apud Quilligan, (3))
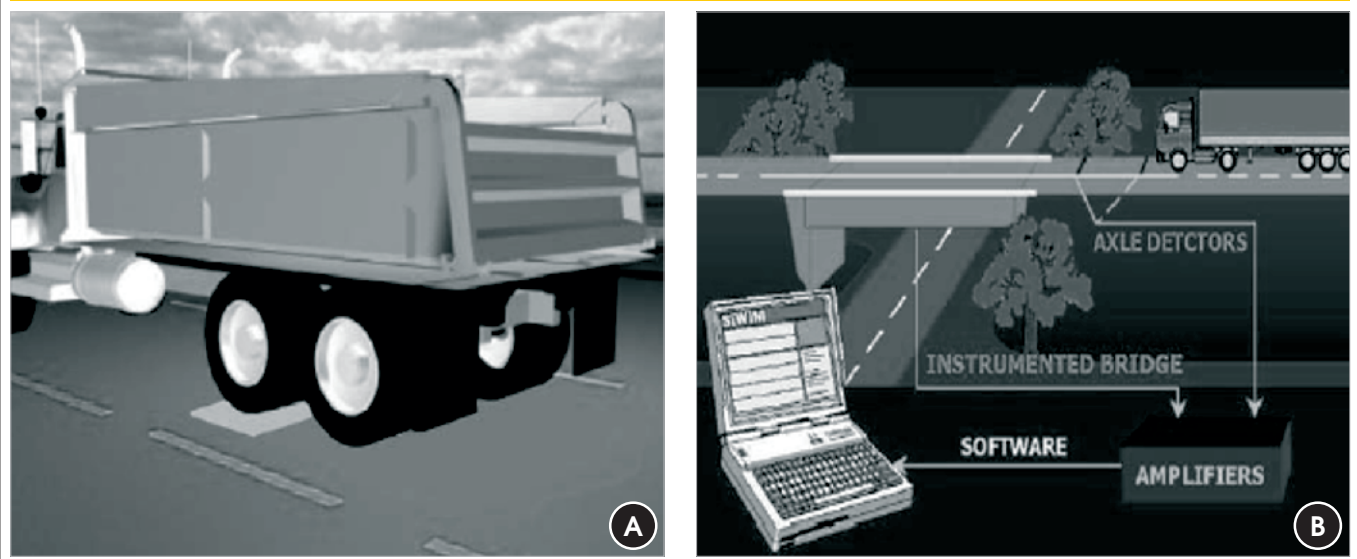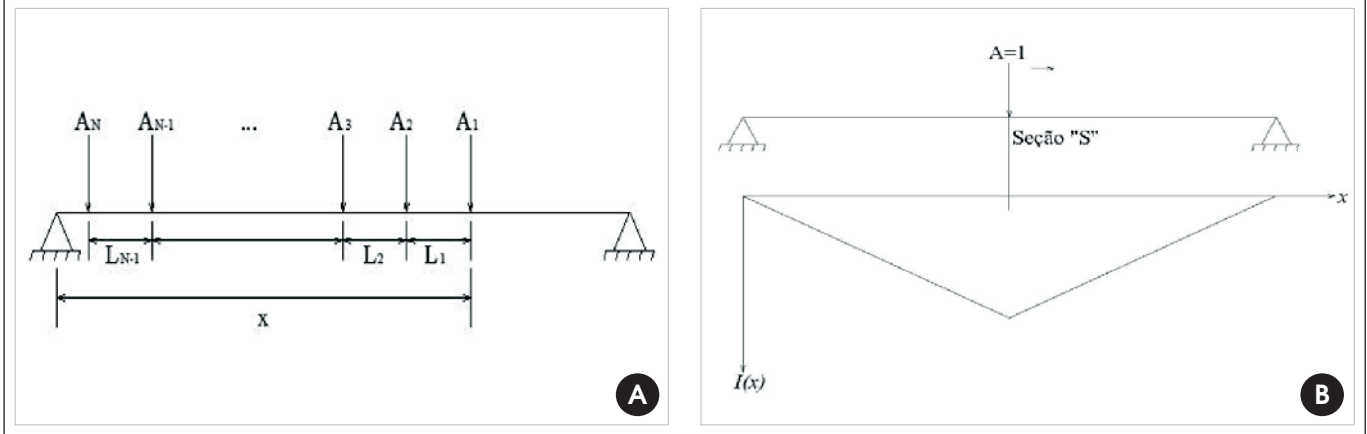
**Figure 2 – a) Position of the axles along the bridge;
b) Influence line of the bending moment**

for the application of the algorithm is the gap between their natural frequency and the frequency of passage of each axle.

$$f = \frac{V}{d_{axles}}$$ (1)

There are other factors that may decrease the precision of the method, such as the difficulty in the determination of a proper influence line and the variation in the velocity during the passage of the vehicle.

The influence line must take into account the elements of the bridge, like sleepers, ballast, tracks and load spreading. Therefore, it is necessary, for a numerical or experimental verification, that the most appropriate influence line is achieved.

The algorithm has two inputs: the time-series of the bending moment of a determined transversal section of the bridge and its respective influence line. The time-series is obtained from the deformations measured with strain-gages, fixed on the main girders of the bridge, and the influence line at that same section.

2.1 B-WIM Algorithm

The algorithm of Moses (Moses [1]) is based on the concept of influence line, in which a moving load over a structure causes reactions proportional to the product of the influence line's ordinate and the magnitude of the respective load. Assuming that the structure has n longitudinal girders, each girder must be instrumentalized in the longitudinal direction at mid-span. For a determined static position of a vehicle, the total bending moment is equal to the summation of the bending moments in each of the girders. Assuming that the structure is under elastic regime, the bending moment may be formulated as a function of its deformation.

$$M_i = f(\varepsilon_i)$$ (2)

Where:

$f(\varepsilon_i)$ is the deformation measured in the girder i.

The algorithm B-WIM is an inverse problem, in which the response is known, being necessary to determine one the variables. Knowing the characteristics of the vehicle, the number of variables of the problem corresponds to the number of axles (N), which can be obtained through the N different values of the bending moment in k different positions of the vehicle on the bridge, see Figure [2]-a. Considering a sampling for the passage of the vehicle over the structure, it is possible to define the bending moment as a function of the time or number of readings. In the same way, knowing the velocity and the spacing between axles, it is possible to define the ordinate of the influence line for each axle as a function of time, see Figure [2]-b. Considering the principle of superposition of effects, the theoretical bending moment is given by:

$$M_k(t_k) = \sum_{i=1}^{N} A_i I_i(t_k)$$ (3)

Where:

$M_k(t_k)$ is the theoretical bending moment at time k;

A_i is the load of the axle i;

$I_i(t_k)$ is the ordinate of the influence line to the axle i at time k.

The results collected from the structure's monitoring are obtained in function of time. By matching the readings of bending moment in the instant k as M_k^*, it is possible to settle the quadratic deviation function E between the theoretical value and the measured value of the bending moment using equation [4].

$$E = \sum_{k=1}^{t_f} \left[M_k(t_k) - M^*(t_k) \right]^2$$ (4)

Where:

t_f is the vehicle's total passage time, or the total time of the signal time increments;

Figure 3 – Numerical model of the WOA 01 (half section)
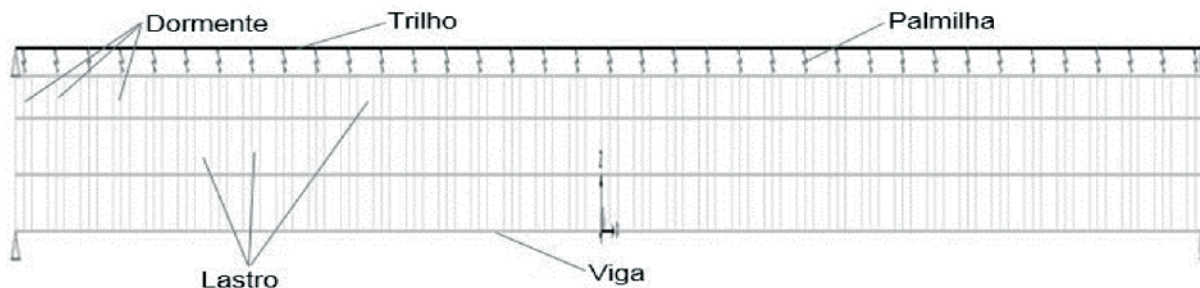
$M^*\left(t_k\right)$ is the bending moment at the instant k.

Since it is willing to calculate the loads, it is needed that the error related to the loads be minimized, verging zero. For this, the partial derivatives of E in relation to each load A_j are set equal to zero, and the matrices $[F]$ and $\{M\}$ are then obtained.

$$[F]=\left[F_{ij}\right]=\sum_{k=1}^{T}I_i\left(t_k\right)I_j\left(t_k\right) \tag{5}$$

$$\{M\}=\{M_j\}=\sum_{k=1}^{T}M^*\left(t_k\right)I_j\left(t_k\right) \tag{6}$$

Where:

$[F]$ is the matrix of the influence line of the bending moments;
$\{M\}$ is built with the bending moments calculated in function of the deformations measured and the influence lines;

T is the total number of instants of time after the reading analysis. In matrix form, the axle loads, A, are given by equation [7]. The gross vehicle weight (GVW) is the summation of the vector {A}.

$$\{A\}=[F]^{-1}\{M\} \tag{7}$$

3. Implementation and numerical validation

Having the algorithm ready, it was needed to validate it, so a bidimensional numerical example was performed. The chosen structure was a reinforced concrete viaduct belonging to the Estrada de Ferro Carajás, managed by the minning company VALE, located near São Luís. The structure was modelled in finite elements using the software SAP2000® [5].

The analysis considered only half of the cross-section of the bridge due its symmetry, see Figure [4]-b, using beam, membrane and spring elements, see Figure [3].

**Figure 4 – a) Overview of the viaduct over the CFN 1st crossing (Carvalho Neto et al (6));
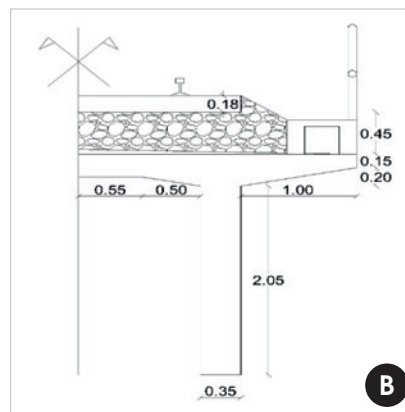b) Half cross-section of the viaduct**

Table 1 – Natural frequencies obtained from the numerical model		
Mode	Frequency (Hz)	Mode shape
1	8.42	Vertical flexure
2	30.21	Vertical flexure
3	36.23	Transversal flexure
4	61.88	Vertical flexure
5	82.63	Transversal flexure

3.1 Description of the viaduct

The viaduct over the CFN 1st crossing corresponds to the work of art number 01 (WOA 01) of the Carajás Railroad, located at the km 4+900. It is a reinforced concrete viaduct with 44.90 m long, constituted by an isostatic span of 18.00 m, a left abutment of 15.25 m and the right one measuring 11.65 m. In Figure [4]-a it is presented an overview of the structure and the cross-section used for data acquirement. Due the symmetry, it was adopted only half cross-section for the modeling in finite elements, as can be seen in the Figure [4]-b.

3.2 Modal analysis

In order to apply the B-WIM system, it is necessary to initially run a modal analysis of the viaduct to determine the modal parameters, which will help the modeling and application of the method.
Having the fundamental natural frequencies of the structure, it can be determined if the B-WIM is applicable, because the existence of regularly spaced axles may cause the phenomenon of resonance or excessive vibration in the structure, where the increasing of velocity is a basic factor for the growth of this frequency, as seen in equation [1].

The modal characteristics of the structure were determined and the first five natural frequencies, referring to the vertical and transversal flexure modes, are presented in Table [1].
Preliminary analysis were made aiming the detection of the most relevant vibration modes of the model, having as parameter the modal influence of the mass, once many modal shapes identified refer to the pads. Figure [5] shows the first two vibration modes obtained.

3.3 Determination of the influence line and the vehicle

For the implementation of the algorithm it was also needed to determine an influence line able to faithfully represent the numerical model and to build the vehicle with axles spacing and loads similar to the operational ones. Thus, it was developed an algorithm that generates linear functions that correspond to the passage of a vehicle in each node of the beam element representing the trail.
The algorithm works by loading the nodes with unitary forces and applying displacements in function of the velocity and the adopted increment. This way, the equivalent functions of these loads due the passage of the loads are obtained. The algorithm assigns the unitary loads through a vector with coefficients related to the axles of the locomotive and wagons, which use the weight variation of the axles.
This algorithm helps in the determination of the influence line in a numerical form, if applied as a vector of unitary coefficients.
Lastly, a time history analysis was performed using the direct linear integration method.

3.3.1 Influence line

The influence line of the bending moment was drawn for the cross-section where the strain-gages were installed, distant 1 meter from the mid-span to velocity of 1 m/s. After the analysis of the model, the results were processed and the influence line in space domain was obtained. Then, the polynomial coefficients used to represent the influence line were determined, see Figure [6].

Figure 5 – a) First vibration mode (f=8.42 Hz); b) Second vibration mode (f=30.21 Hz)

Figure 6– Influence line obtained and curve of the influence line determined
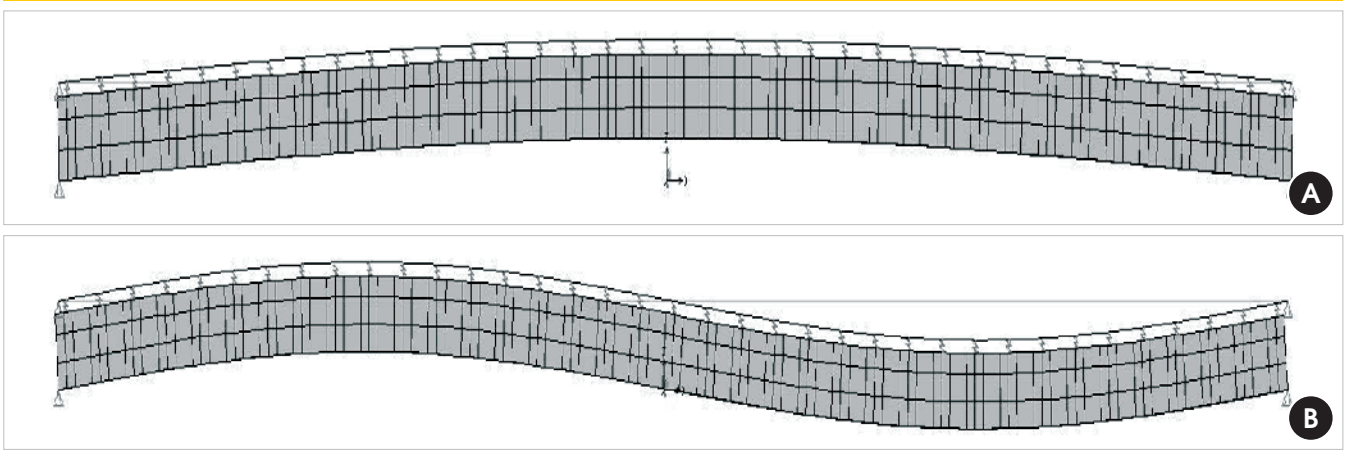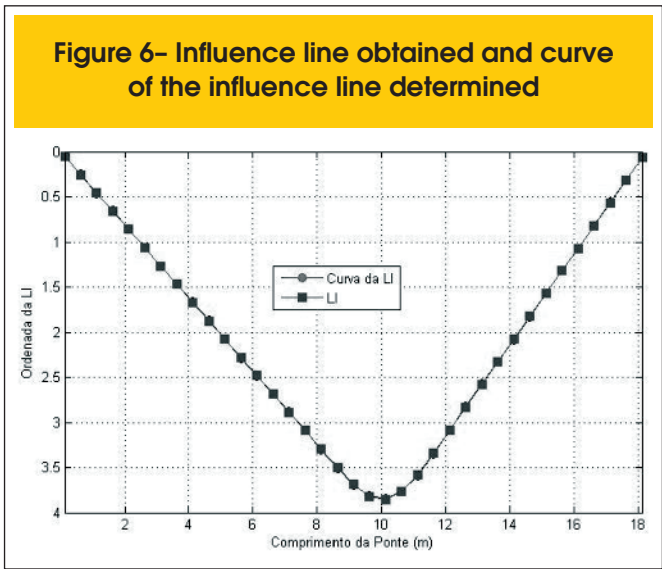
3.3.2 Vehicle

The simulations were made using 6 different velocities (1 m/s, 5, 10, 40, 60 and 80 km/h) for an arrangement of 2 locomotives and 4 wagons, see Figure [7], with axles weighing 300 kN and 325 kN, respectively. It was used the algorithm "Calcula_TimeHistory" to generate the corresponding functions and this way to load the nodes of the computational model in order to obtain a time series of the bending moments of the section equivalent from which was withdrawn at the influence line.

Once in possession of the time-histories, it is important to verify the difference between the natural frequencies and the static part of the response, since the frequencies related to the axles spacing must not be within the natural frequencies. Table [2] presents the

maximum calculated frequencies for the adopted number of passages and, thus, it is concluded that there is no dynamic interference between the natural frequencies and the ones determined.
In Figure [8], the treated time history is presented in which a moving average of seventh order and a low-pass digital filter with threshold of 8 Hz was used, inferior to the first natural frequency (8.42 Hz).

3.4 Results

In possession of the bending moment's time-series and the influence line, the axle loads for the previously mentioned velocities were calculated (Figure [9]). For better analysis of the results, the mean errors for the axle loads (Figure [10]) and GVW (Table [3]) were calculated.
Table [3] presents the calculated values for gross vehicle weight (GVW), which achieved minimum differences in comparison with the vehicle's actual value (8800 kN), even in face of larger discrepancies between the axle loads. Regarding the axle loads of Figure [9], they presented a small variance in comparison with their real values, stressing that the results for a passage of the train for the velocities of 60 km/h and 80 km/h showed values around the actual ones.
The average error of the loads and the error of the total gross weight were calculated using the Equations [8] and [9], respectively.
In Figure [10], it is verified that the relative error is smaller for lower velocities due the reduced dynamic effects. For velocities up to 40 km/h, the maximum error reached 10 %, referring to the fourth axle of the first locomotive of the arrangement (2 locomotives and 4 wagons). The maximum relative errors found for 60 km/h and 80 km/h were 12 % and 18 %, respectively. From Figures [9] and [10], it is observed that the calculated axle loads were distributed unequally, producing average mean errors varying from 3.16% (1m/s) to 9.82 % (80 km/h). However, the achieved GVWs presented errors smaller than 1% for every velocity.

Figure 7 – Arrangement of 2 locomotives and 4 wagons adopted in the numerical example
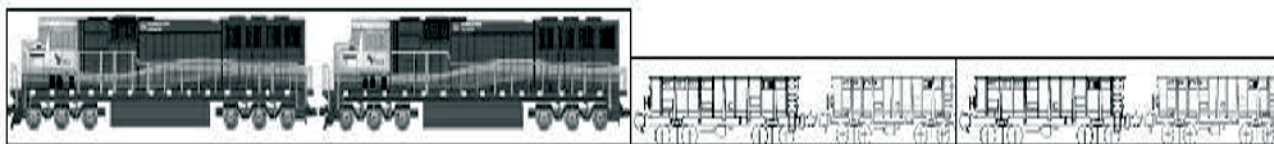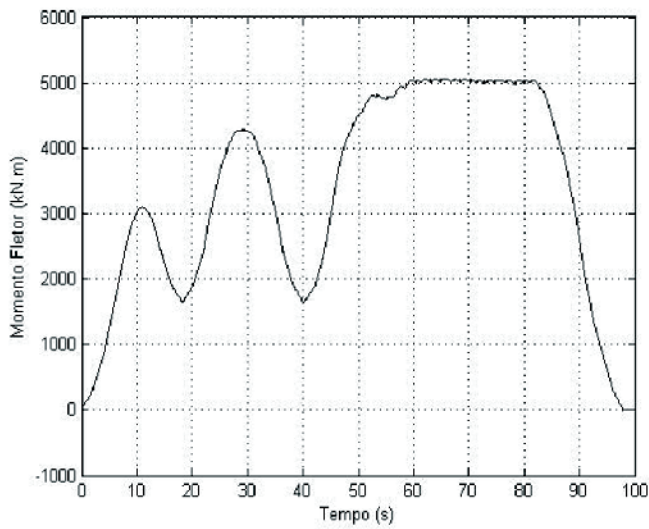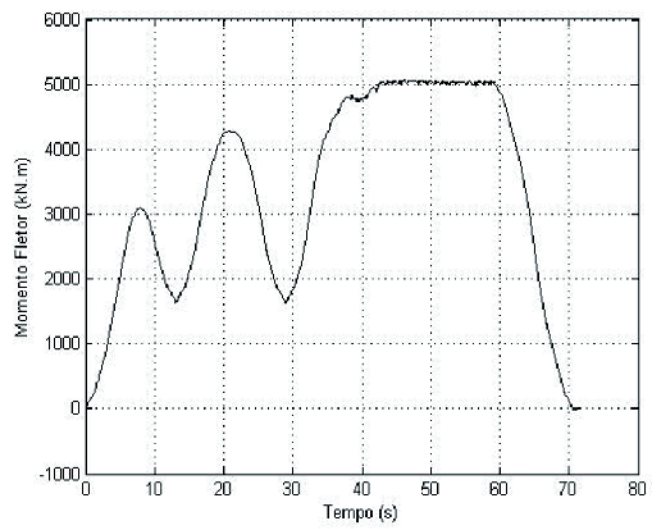

Table 2 – Frequencies related to the distance between axles for varying traffic velocities

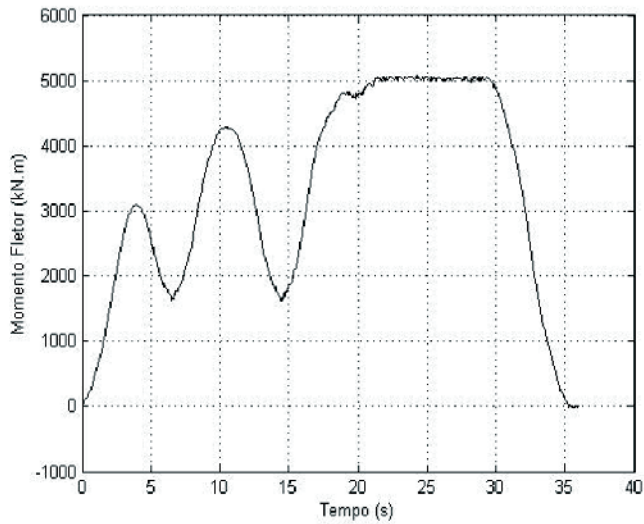| Vehicle	Frequencies (Hz)					
	80 km/h	60 km/h	40 km/h	10 km/h	5 km/h	1 m/s
Locomotive	1.56	1.17	0.78	0.19	0.10	0.07
Wagon	4.15	3.11	2.07	0.52	0.26	0.19

Figure 8 – Time-histories of the bending moment in the girder:
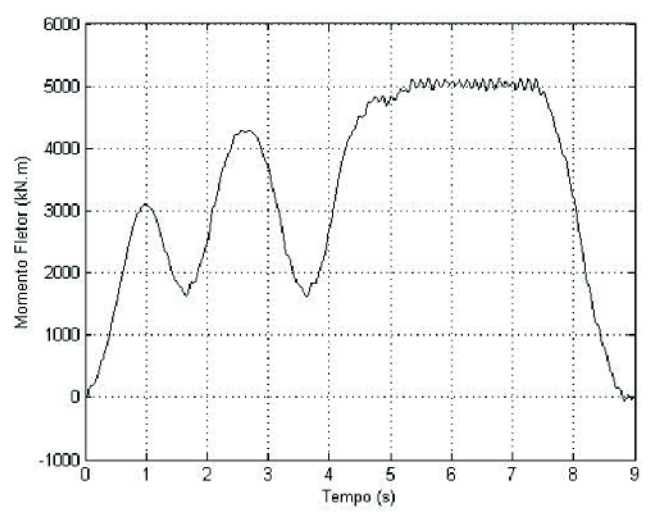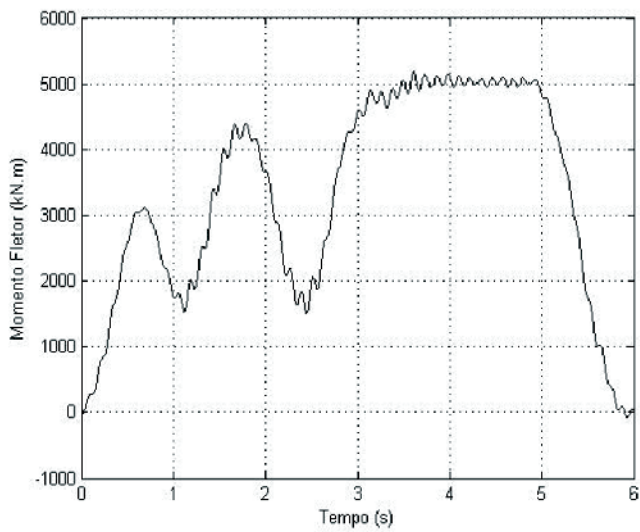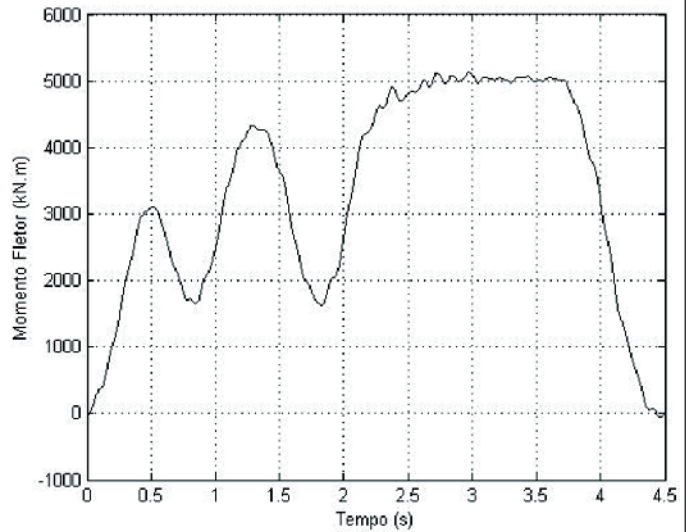**a) 1 m/s; b) 5 km/h; c) 10 km/h; d) 40 km/h; e) 60 km/h; f)80 km/h**

**Figure 9 – Axle loads determined by the algorithm of Moses (1) for velocities:
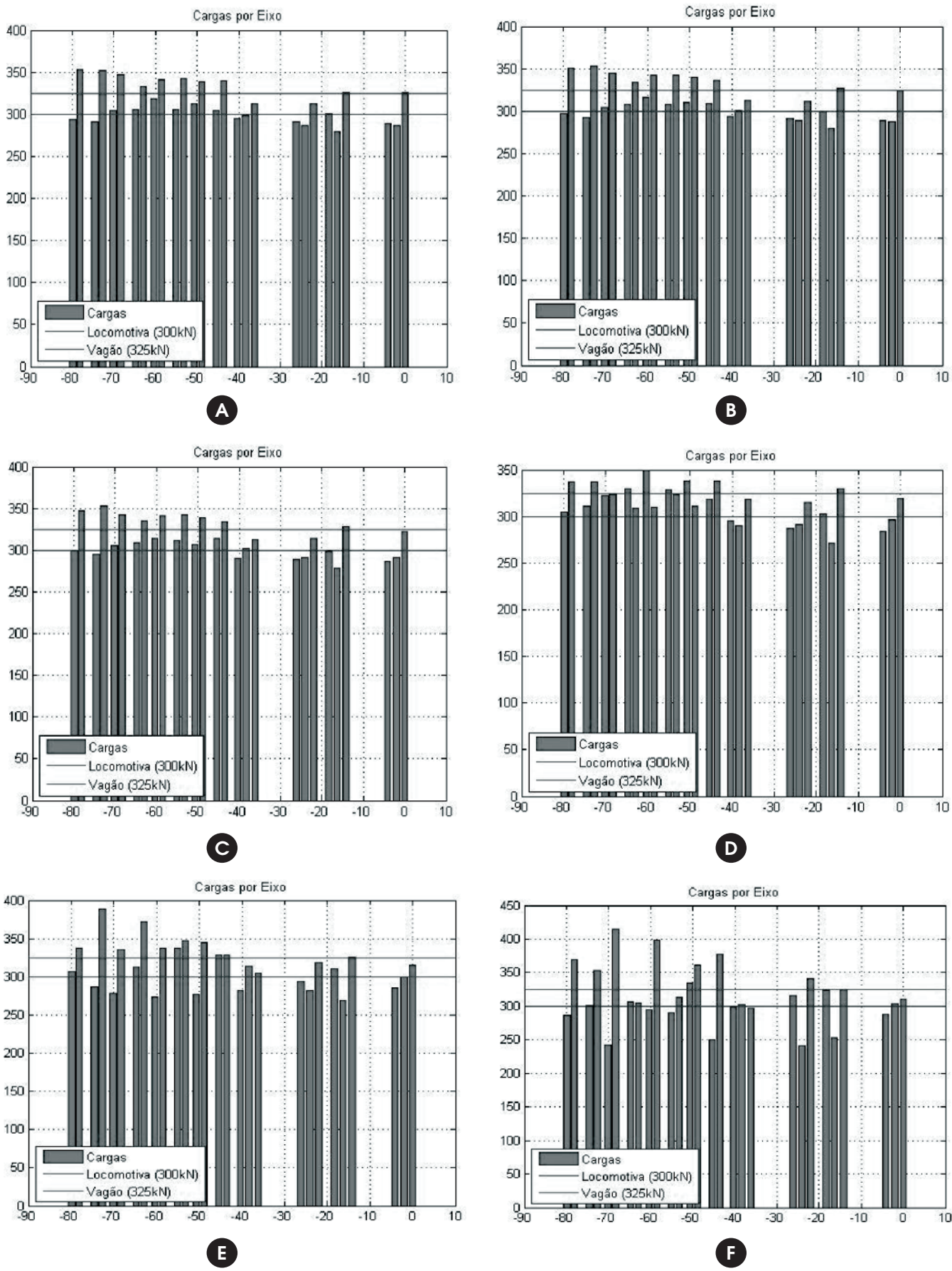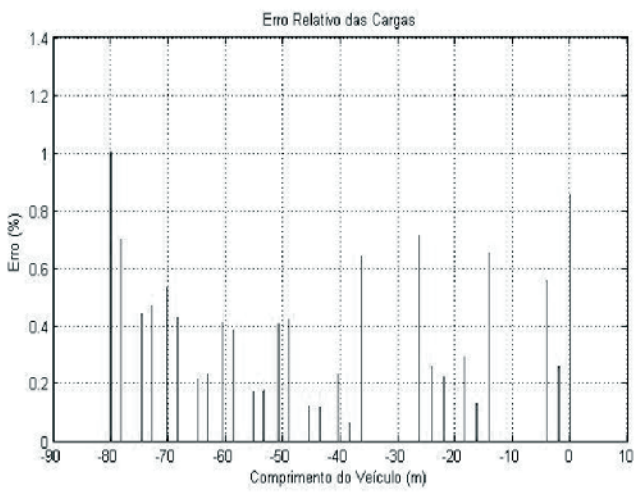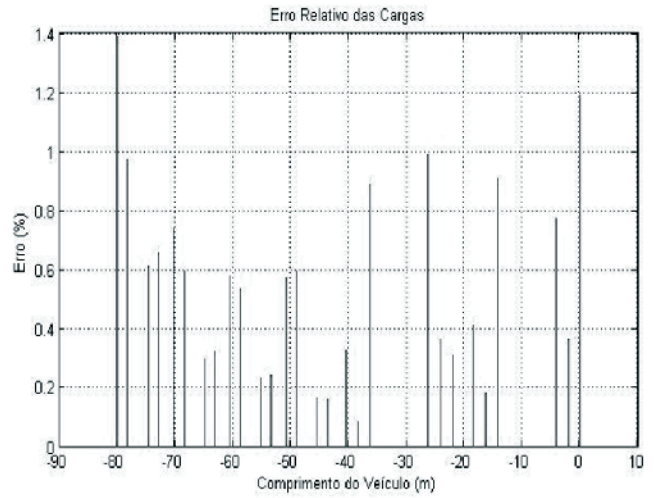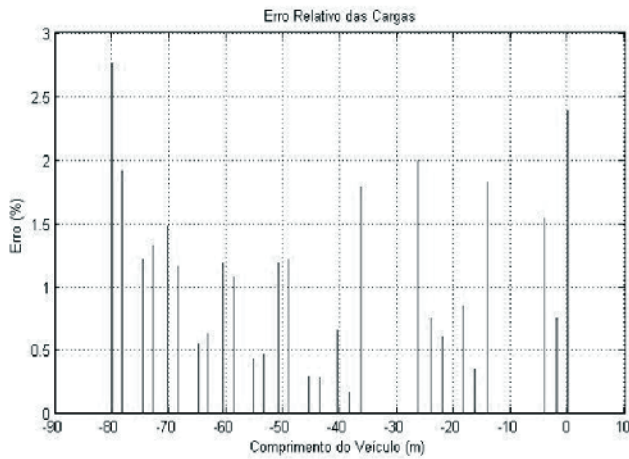a) 1 m/s; b) 5 km/h; c) 10 km/h; d) 40 km/h; e) 60 km/h; f) 80 km/h. Values in kN**

Figure 10 – Errors per axle determined for varying velocities: a) 1m/s; b) 5km/h; c) 10km/h; d) 40 km/h; e) 60 km/h; f) 80 km/h

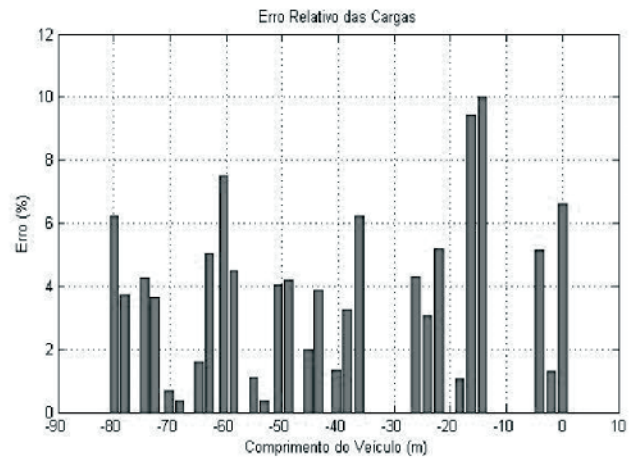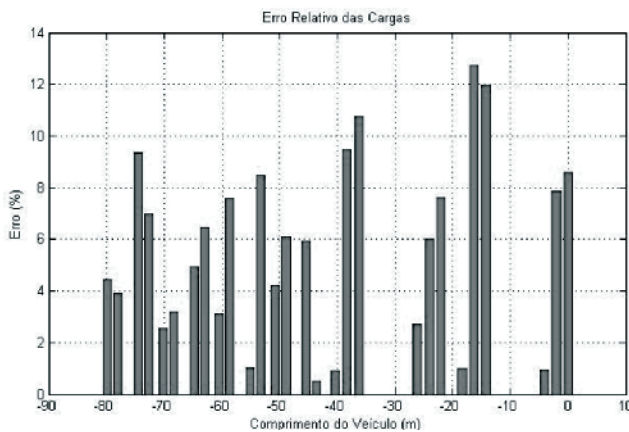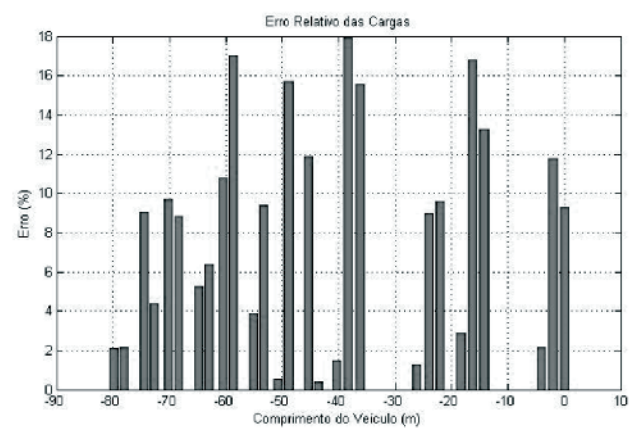| Table 3 – Total gross weight error and average axle load error for varying velocities						
Total gross vehicle weight error and average axle load error (%)						
Error/Velocity	80km/h	60km/h	40/km/h	10km/h	5km/h	1m/s
GVW	0.05	0.05	0.06	0.07	0.08	0.11
Average	9.82	6.24	4.73	4.44	4.22	3.16

4. Characterization and weighing of a locomotive from experimental data

After benchmarking the algorithm, a field trip was done to weigh and characterize the train from experimental data. The actual structure used in the procedure was the same one used in the numerical model, see Figure [4]-a.

4.1 Instrumentation of a viaduct

The instrumentation of the viaduct was made near its midspan and at the expansion joints, see Figure [11], located at its entrance and exit. Due the presence of a girder at midspan, two strain-gages were installed far 1m from it in the longitudinal direction, in the lower reinforcement and over the viaduct, directly on the concrete surface, see Figure [11]. The models were KFG, from KYOWA, which are proper for outdoor use.

In order to fix the strain-gage on the concrete, it was necessary to remove parts of the mortar layer and ballast of the railroad, and to fix another on the lower reinforcement, part of the concrete was removed.

4.2 Data acquisition

The ADS-2000® system was used to collect the data from the strain-gages. An ethernet network was set up between the system and a computer, see Figure [12]. The data was collected under a 100 Hz rate.

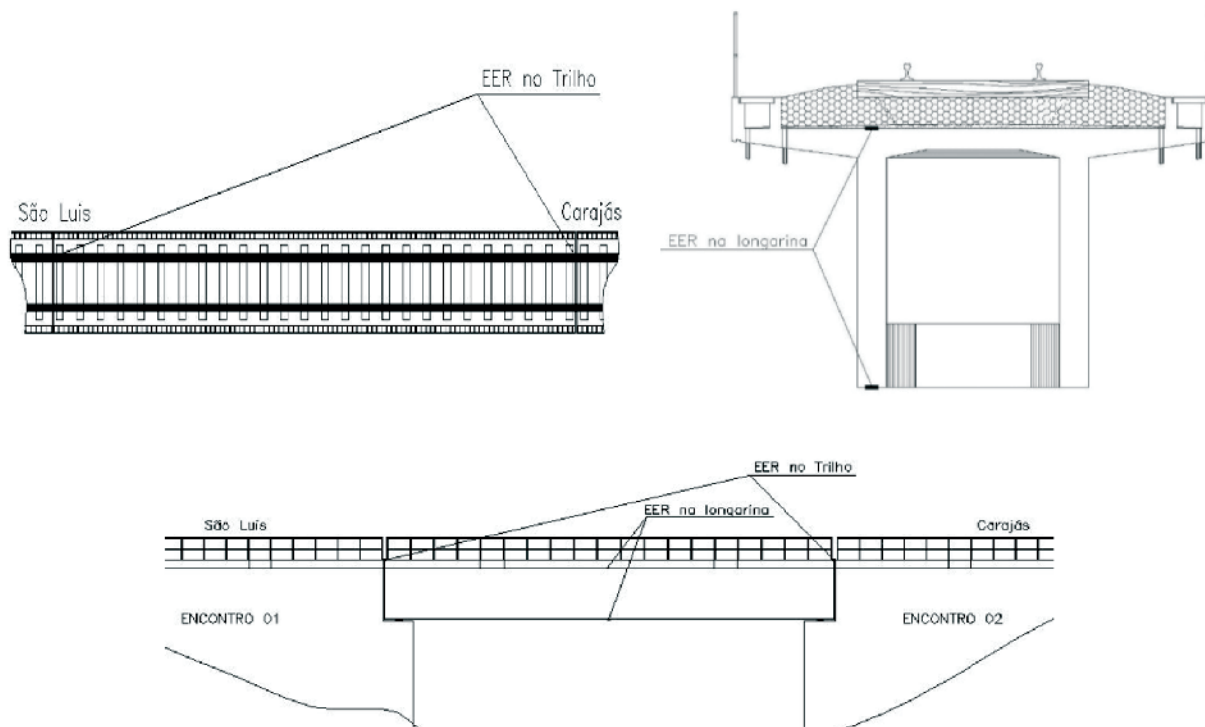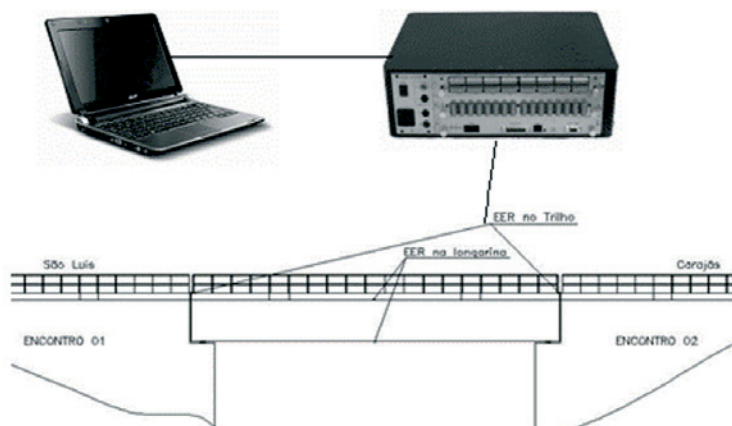**Figure 11 – Strain-gages fixed on the trails and girders**

Figure 12 – Draft of the data acquisition's setup

4.3 Peak Detection

The peak detection is a crucial step for the definition of the vehicle's geometry. The passage of a vehicle's axle over an instrumentalized section creates a peak in the time-series of deformation, which allows the knowledge of the quantity and spacing of axles. Thus, it is needed to distinguish what is a peak. For that, it was used the algorithm "peakfinder" (Yoder [7]), developed in MATLAB language (MATLAB [8]), which has inputs:
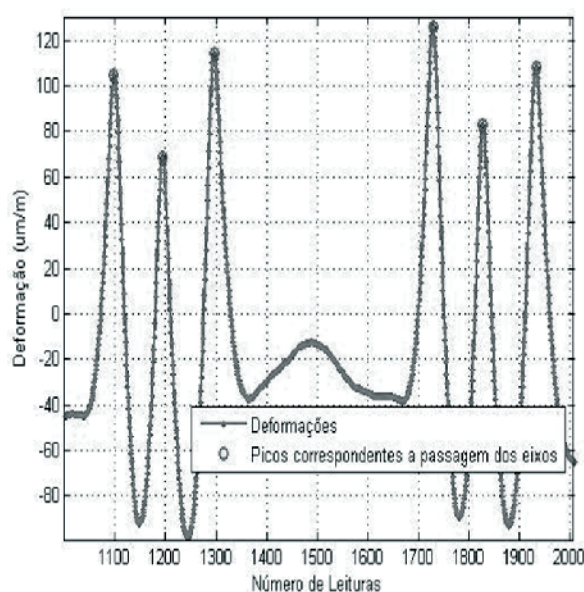a) The time-series vector;
b) A threshold;
c) An extreme: 1 when searching for maximum, -1 when searching for minimum.
The outputs are the peak values and their respective time of

Figure 13 – Maximum detected in the time-series of deformation of the trail under the passage of a locomotive a) Strain-gage installed on São Luis' side; b) Strain-gage fixed on the Carajás' side
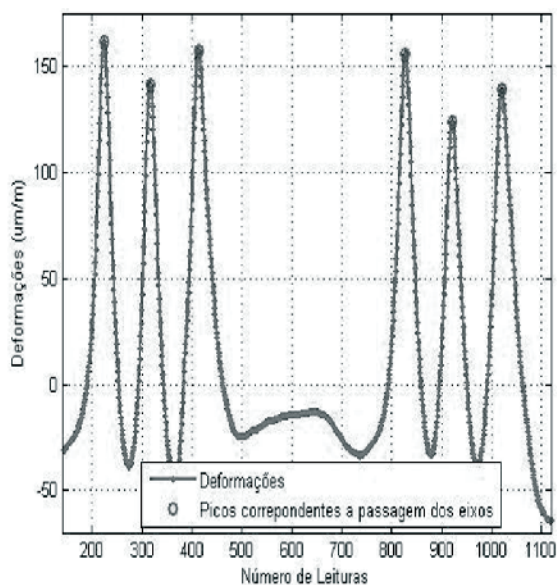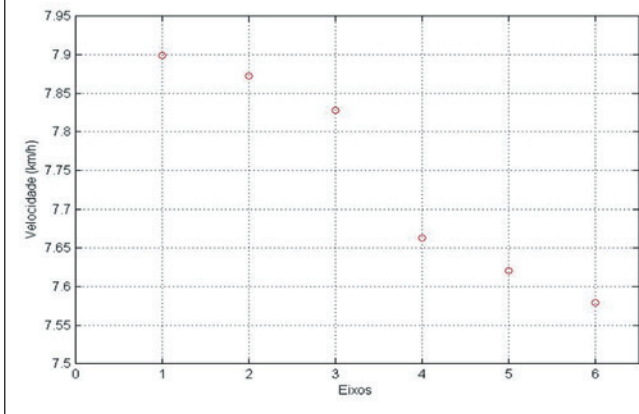
Figure 14 – Speed per axle obtained from a deformation time-series due the passage of a DASH-9 locomotive at midspan

Table 4 – Comparison of actual and calculated axle spacing

Real distance (m)	Obtained distance (m)	Difference (m)
0	0	0
2.0193	2.0324	0.0131
2.1209	2.1198	0.0010
10.0838	9.0475	1.0362
2.1209	2.0542	0.0666
2.0193	2.1854	0.1661

occurrence (in seconds). Figure [13] presents the peaks, or axles, obtained from the experimental data. It is clear the presence of six peaks, corresponding to the passage of the six axles of the locomotive over the trails instrumentalized on the sides of São Luis and Carajás, respectively.

The time interval between the passages of the same axle over distinct sections is calculated based on the variation of the reading numbers among the samples divided by the sampling rate of the data acquisition, fixed in 100 Hz.

4.4 Calculation of axles' speed and spacing

The speed calculation per axle was made using the Rectilinear Motion formulation. Then, the average speed of the locomotive was achieved, see Figure [14].

The average speed obtained was 7.74 km/h for the analyzed signal. Using the average speed and the maximum peaks, it was possible to calculate the locomotive axle spacing. In Table [4], the values of the calculated axle spacing and their actual values are presented. The values obtained are close to the actual ones. To perform this analysis, it were used the axle spacing of the locomotive type DASH-9, the most used by the VALE mining company, although it also works with locomotives with varying axle spacing.

4.5 Obtaining the Bending Moment's Time-Series

The obtainment of the bending moment's time-series was performed using constitutive models for the bridge materials and the Navier-Bernoulli Hypothesis.

4.5.1 Constitutive models

The deformation's time-series provided by the strain-gages must be converted in bending moment's time-series. For that, it was necessary to study the mechanical behavior of reinforced concrete and to define the relations between its stresses and deformations. These relations were defined based on the constitutive models for

the steel and concrete and the Navier-Bernoulli Hypothesis.

4.5.1.1 Constitutive models for the concrete

There are several models to represent the mechanical behavior of concrete, consisting in relations between its stresses and strains. The linear-elastic model is the simplest. The plastic model is another very used one, been characterized by the occurrence of residual deformations when unloaded. In this paper, it were adopted elastic non-linear models.

4.5.1.1.1 CONSTITUTIVE MODEL FOR THE CONCRETE (ABNT NBR 6118 [9])

a) Compression

Under compression, to analyze the ultimate strength limit, it may be used the idealized stress-strain diagram presented in Figure [15].

The constitutive equation for the concrete under compression is presented in equation [8].

Figure 15 – Idealized Stress-strain diagram (ABNT NBR 6118 (9))

$$\sigma_c = f_{ck}\left[1-\left(1-\frac{\varepsilon_c}{2\permil}\right)^2\right]$$
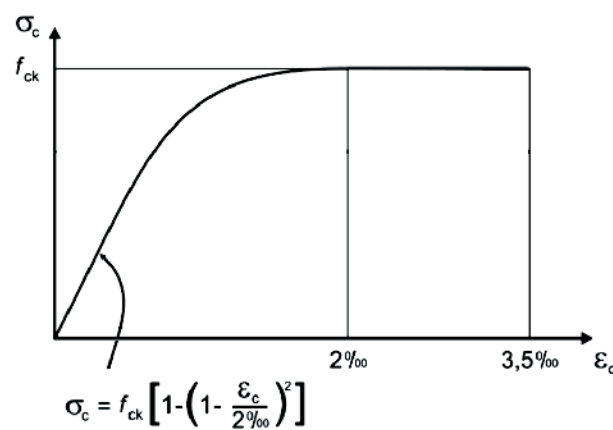
$$\sigma_c = 0,85\,f_{ck}\left[1-\left(1-\frac{\varepsilon_c}{0,002}\right)^2\right] \text{ if } 0=\varepsilon_c=0.002$$

$$\sigma_c = 0,85\,f_{ck} \text{ if } 0,002<\varepsilon_c=0.0035$$

$$\sigma_c = 0 \text{ if } \varepsilon_c>0.0035$$

(8)

Where:

σ_c Is the compression stress;

f_{ck} Is the compression's ultimate strength of the concrete obtained from specimen compression tests;

ε_c Is the concrete's strain.

b) Tension

Under tension, the brazilian standard considers the strength of the concrete equals 0 (zero), when cracked. In the algorithm, the main girders were considered all cracked along their longitudinal direction, causing the concrete's resistance in tension to be null.

4.5.1.1.2 Constitutive models (Collins and Mitchell [10])

a) Compression

The model proposed presents a family of curves for the behavior of concrete under compression and tension (Collins and Mitchell [10]). The performance of the concrete under compression is described by the equation [9].

$$\sigma_c = f_{ck}\cdot\left[\frac{n\left(\dfrac{\varepsilon_c}{\varepsilon_{ck}}\right)}{n-1+\left(\dfrac{\varepsilon_c}{\varepsilon_{ck}}\right)^{nk}}\right] \text{ if } \varepsilon_c=0$$

(9)

Where:

σ_c Is the compression stress;

f_{ck} Is the compression's ultimate strength of the concrete obtained by sample tests;

$n = 0,8+\dfrac{f_{ck}}{17}$ With fck in MPa;

ε_c Is the concrete's strain;

$\varepsilon_{ck} = \dfrac{f_{ck}}{E_c}\cdot\dfrac{n}{n-1}$ Is the deformation of the concrete corresponding to its maximum stress;

$k = 0,67+\dfrac{f_{ck}}{62}\geq 1$ With fck in MPa.

b) Tension

The curve that represents the concrete behavior under tension simulates the resistance contribution between cracks ("tension-stiffening" effect). When over the cracking strain (ε_{cr}), the concrete still presents strength due the bond between its intact portions and

the reinforcement, which transfers to the concrete its stress through radial forces. The post-cracking response of the tensioned material is considered in a way that the axial load is shared by both concrete and steel along the length of the element, (Rêgo [11]). The tension stress in the reinforcement will be greater in the cracked section than in its neighborhood, once the strees in the concrete is null on that section. In the traditional processes, this superposition is neglected, than the reinforcement's response is taken as if it was uncovered in its extension. The model estimates the average contribution of the concrete in tension, following many other papers, which also propose constitutive equations based on experimental results.

The performance of the concrete under tension is described by the equation [10].

$$\sigma_c = \frac{\alpha_1\alpha_2}{1+\sqrt{500.(-\varepsilon_c)}} \text{ if } \varepsilon_c<0 \;\&\; \varepsilon_c<\varepsilon_{cr}$$

$$\sigma_c = E_c.\varepsilon_c \text{ if } \varepsilon_c<0 \;\&\; \varepsilon_c=\varepsilon_{cr}$$

(10)

Where:

σ_c Is the compression stress;

ε_c Is the concrete's strain;

$E_c = 3320+\sqrt{f_{ck}}+6900$, In MPa, is the elastic modulus proposed;

α_1 Is a coefficient relative to the bonding between the reinforcement and the concrete (equals 1.0 for ribbed, 0.7 for smooth bars or strands and 0 for loose bars);

α_2 Is a coefficient relative to the type of load (equals 1.0 for monotonic loading of small duration and 0.7 for cyclic or long duration loading).

4.5.1.2 Constitutive model for the steel

In reinforced concrete structures, the reinforcement is used to contribute only for axial loading, and so it is only needed to know the uniaxial properties of the material in order to properly model it. The presence of a constant yielding stress in the stress-strain curve depends on the manufacturing process of the steel. The present model possession it (Teixeira [12]).
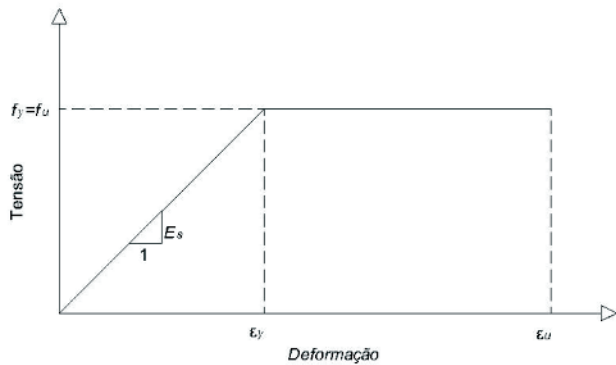
4.5.1.2.1 Perfectly elastoplastic model

The perfectly elastoplastic behavior is presented in Figure [16]. The relation is given by the equation [11].

$$\sigma_s = E_s.\varepsilon_s \text{ if } \varepsilon_s=\varepsilon_y$$

$$\sigma_s = f_y \text{ if } \varepsilon_s=\varepsilon_y \;\&\; \varepsilon_s=\varepsilon_u$$

$$\sigma_s = 0 \text{ if } \varepsilon_s=\varepsilon_u$$

(11)

4.5.1.3 Experimental load acquisition

To determine the bending moment's time-series, it was performed the methodology based on the Navier-Bernoulli beam hypothesis,

Figure 16 – Steel's stress-strain diagram in reinforced concrete

Table 5 – Comparison of calculated and actual "GVW" of the locomotive

PBT real	PBT (NBR 6118/2007 (9))	PBT (Collins & Mitchell (10))
1800 kN	1425.57 kN	1768.61
Erros	20.80%	1.74%

σ_f is the stress on the fiber;
y_f is the height of the fiber j
Figure [19] presents the flowchart for the calculation and storage of the loads used.
Figure [20] presents the bending moments' time-series from the adopted constitutive equations.

4.6 Axle loads and gross-vehicle-weight

Having all the inputs, the locomotive's axle loads were calculated using both constitutive equations. Due the absence of an experiment with a known weight vehicle, it was adopted an influence line for a 1 m/s speed, once it causes a negligible dynamic effect.
In two occasions, negative axle loads were found. Even when considering their absolute values, they present great distance from the actual ones (300 kN/axle). By observing Table [5], it is concluded the calculated gross weight are much closer to its actual values when the constitutive equations are used (Collins and Mitchell [10]).

which considers that the initial parallel sections of the beam remain parallel after the load is applied and normal to the beam's axis (Pureza [13]). Adopting the joint behavior of steel and concrete, then the strain in some point of the section is equal for both materials. Using this result and by assigning the centroid (centre of gravity) of the section as a fixed reference line, it is possible to determine the deformation in every point of the section, see Figure [17]. For the evaluation of the concrete, it was used the model beams with section discretization in fiber, consisting on the discretization of the cross-section in fibers parallel to a reference axis of constant thickness, see Figure [18], considering that the strain on every point of a fiber is constant. The stresses were obtained from the constitutive material equations previously described. With the stress in each fiber and reinforcement layer j, we are able to calculate the loads in every instant i, and the bending moment's time-history will be the summation of the bending moments of each fiber and reinforcement layer.

$$M_{i,j} = A_{f_j} . \sigma_{f_{i,j}} . y_{f_j} \tag{12}$$

Where:
A_f Is the area of the fiber;

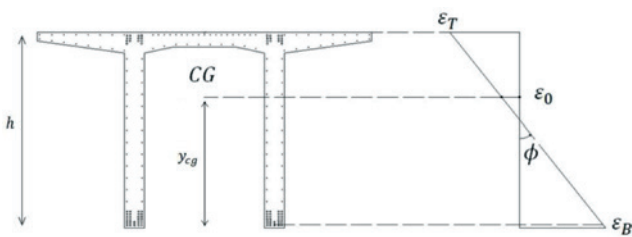**Figure 17 – Strain distribution along the height of the section (Pureza, (13))**

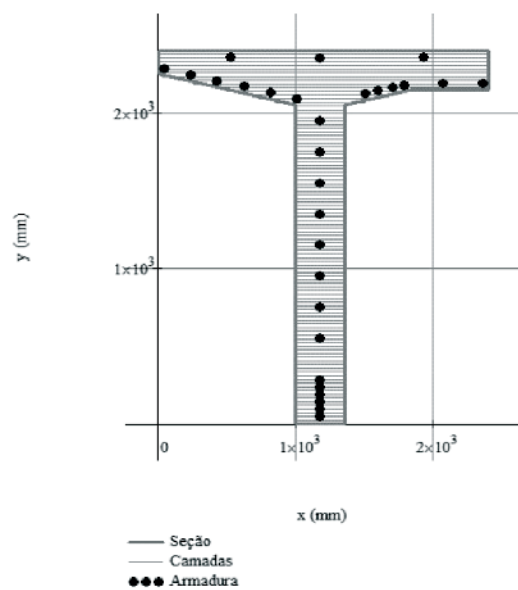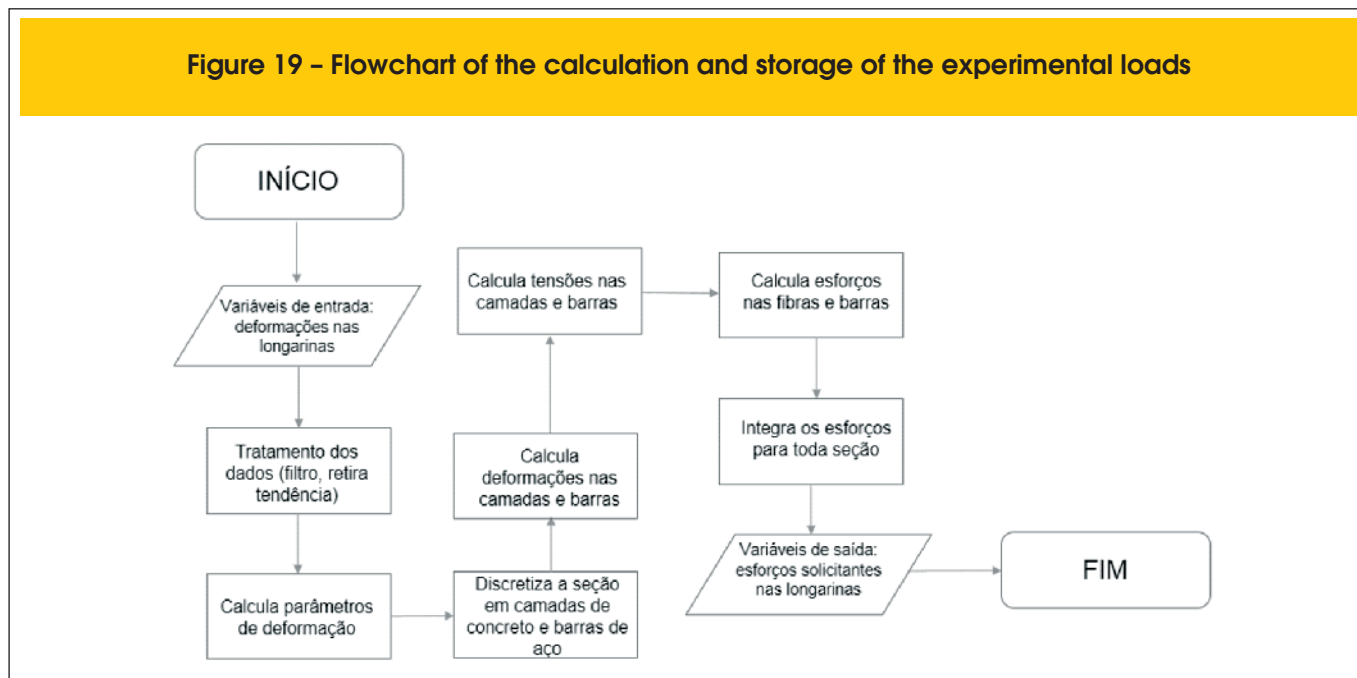**Figure 18 – Cross-section in fibers and reinforcement**

Figure 19 – Flowchart of the calculation and storage of the experimental loads

5. Conclusion

The axle detection proved very effective, easily identifying the passage of all the axles expected from the time-series.

The bending moments time-series allow the evaluation of the performance of the constitutive equations adopted for the concrete. The best results were achieved using the constitutive model (Collins and Mitchell [10]), proving that it is the most appropriate model for the present problem.

The algorithm used for the identification of axle loads revealed itself very sensitive, once small variations in the inputs lead to large output errors, leading to an average variation of 7.11% for axle loads and 0.03% for the GVW in the numerical example. For the experimental case, the results vary greatly from the actual values, even reaching negative values, but the total gross weight achieved presented an error of only 1.74%.

6. Acknowledgement

Figure 20 – Bending moments' time-series at midspan. a) Using the equation proposed by ABNT NBR 6118 (9); b) Using the equation proposed (Collins e Mitchell (10))
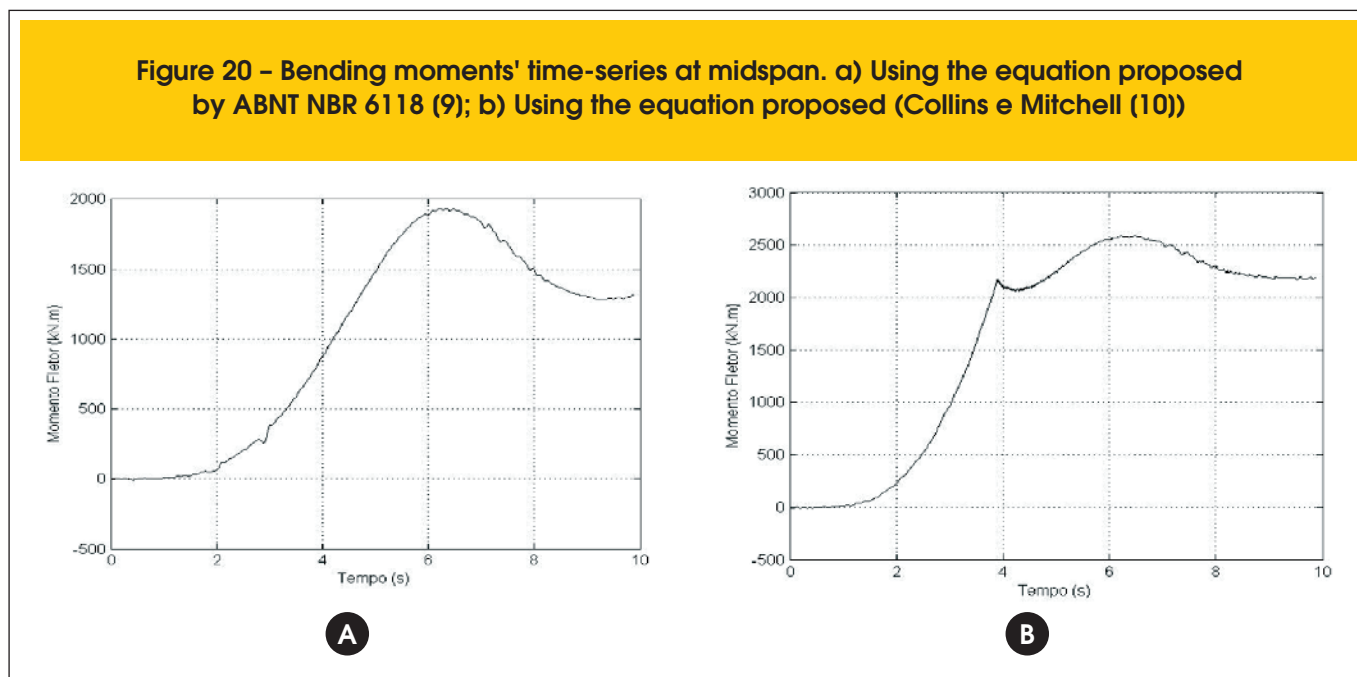
7.   References

[1]   MOSES, F. Weigh-in-Motion System Using Instrumented Bridges. Transportation Engineering Journal, v. 105, n. TE3, 233-249, May 1979.

[2]   ZNIDARIC, A.; BAUMGÄRTNER, W. Bridge Weigh-in-Motion Systems – an Overview. In: PRE-PROCEDINGS OF 2nd EUROPEAN CONFERENCE ON WEIGH-IN-MOTION OF ROAD VEHICLES, 1998, Lisbon.

[3]   QUILLIGAN, M. Bridge Weigh-In-Motion - Development of a 2-D Multi-Vehicle Algorithm. 2003. 162 f. Licentiate Thesis – Department of Civil and Architectural Engineering, Structural Design and Bridge Division, Royal Institute of Technology, Stockholm, 2003.

[4]   PIMENTEL, R. M. C. M. Caracterização do Tráfego Ferroviário e dos seus Efeitos em Pontes de Pequeno Vão. 2008. 188 f. Dissertação (Mestrado em Estruturas de Engenharia Civil) - Faculdade de Engenharia, Universidade do Porto, Porto, 2008.

[5]   SAP2000 Advanced 14.1.0 – Structural Analysis Program, ©1976 – 2009, Computers and Structures, Inc, University Ave. Berkeley, CA, EUA.

[6]   CARVALHO NETO, José A. de; PUREZA, Dennis Q.; COSTA, Fábio I. B. da; VELOSO, L. A. C. M.; SAMPAIO, Regina A. C.; RODRIGUES Jr, Sandoval J.; BARICHELLO, César V. M.; MOREIRA, Jouberson L. da R. Desenvolvimento de Metodologia para Avaliação da Integridade Estrutural de Pontes e Viadutos Ferroviários ao Longo da Estrada de Ferro Carajás. Pará: NICAE-UFPA, 2009. 143 p. (Relatório Técnico Segunda Etapa: Obra de Arte Especial n. 01 - Viaduto sobre a Primeira Travessia).

[7]   YODER, N. PeakFinder. http://www.mathworks.com, acessado no dia 19 de Abril de 2013.

[8]   MATLAB - Matrix Laboratory R2012b 8.0.0.783 ©1984 - 2012, Mathworks, Inc, 3 Apple Hill Drive, Natick - MA, EUA.

[9]   ASSOCIAÇÃO BRASILEIRA DE NORMAS TÉCNICAS. NBR 6118: Projetos de Estruturas de Concreto Armado. Rio de Janeiro, 2007.

[10]   COLLINS, M. P.; MITCHELL, D. Prestressed Concrete Structures. New Jersey, Prentice Hall, 1991.

[11]   RÊGO, G. M. Desempenho dos Modelos da NBR 6118 para Análise de Vigas Contínuas em Concreto Armado. (Dissertação de Mestrado). Programa de Pós-graduação em Engenharia Civil, Universidade Federal de Pernambuco, Recife, 2005.

[12]   TEIXEIRA, Ritermayer M. Estudo Teórico-Experimental do Comportamento Estrutural de uma Ponte Ferroviária em Concreto Armado. 2009. 199 f. Dissertação (Mestrado em Engenharia Civil) – Coordenação dos Programas de Pós-Graduação de Engenharia, Universidade Federal do Pará, Belém, 2009.

[13]   PUREZA, Dennis Q., Avaliação de Segurança de Longarinas de Pontes Ferroviárias em Concreto Armado a partir de Dados Experimentais. 2013. 71 f. Dissertação (Mestrado em Engenharia Civil) – Coordenação dos Programas de Pós-Graduação de Engenharia, Universidade Federal do Pará, Belém, 2013.

[14]   ASSIS, W.S.; TRAUTWEIN, L. M.; BITTENCOURT, T. N.; CONCEIÇÃO NETO, A. P. Structural health monitoring of a steel railway bridge on the river Suaçuí. In: IABMAS 2012 - 6th International Conference on Bridge Maintenance, Safety and Management, Stresa - Itália. Bridge Maintenance, Safety and Management. Leiden - Holanda: CRC Press, 2012. v. 1.

[15]   CHOPRA, Anil K. Dynamics of Structures: theory and applications to earthquake. Englewood Cliffs: Prentice Hall, 1995.

[16]   CLOUGH, Ray W.; PENZIEN, Joseph. Dynamics of Structures. Berkeley: Computers & Structures, 2003.